Hindawi
Advances in Meteorology
Volume 2019, Article ID 8571430, 13 pages
https://doi.org/10.1155/2019/8571430

*Research Article*

# Observation and Real-Time Simulation of a Tornado Event in Hong Kong on 29 August 2018

**K. K. Hon**,[1] **S. M. Tse**,[1] **P. W. Chan**,[1] **and Q. S. Li**[2]

[1]*Hong Kong Observatory, Tsim Sha Tsui, Hong Kong*
[2]*Department of Architecture and Civil Engineering, City University of Hong Kong, Kowloon Tong, Hong Kong*

Correspondence should be addressed to P. W. Chan; pwchan@hko.gov.hk

Received 3 October 2018; Revised 12 December 2018; Accepted 20 December 2018; Published 22 January 2019

Academic Editor: Tomeu Rigo



An observational and simulation study of a tornado event in Hong Kong that occurred in the morning of 29 August 2018 is documented in this paper. Rotating airflow associated with the tornado is well captured by the Doppler velocity from a Terminal Doppler Weather Radar (TDWR) in Hong Kong. The Doppler velocity patterns show the typical signature of a velocity couplet associated with a meso/microcyclone, and for most part of its lifetime, it captures clearly the evolution with time. Weather radar echoes of those thunderstorms inducing the current tornado, as well as the meso/microcyclone itself, are also successfully reproduced in a real-time simulation by a fine-resolution numerical weather prediction (NWP) model initialised 3 hours earlier, albeit with a time lag of about 15 minutes when compared to the actual event. The model simulation displays some interesting features of the cyclone, including the vertical structure of horizontal and vertical velocities and cloud liquid water content, which are consistent with literature that accounts in other parts of the world. The vertical profile of maximum radial velocity associated with the velocity couplet also compares well between the actual weather radar observation and numerical simulation. The results in this paper could serve as an interesting reference for both meteorologists and wind engineers, also demonstrating the power of very high-resolution NWP in predicting such events in a real-time fashion.

## 1. Introduction

Tornado is a rather rare weather phenomenon in Hong Kong. Hong Kong is located over Pearl River Delta, southern China, with a population of about 7.8 million, with subtropical climate. Hong Kong has complex terrain and land-sea distribution, but the geographical conditions do not appear to favour the occurrence of tornadoes in specific regions in the territory. Over south China coast, it is frequently under the influence of tropical cyclones and occasionally there may be tornado occurrence associated with outer rainbands of tropical cyclones (e.g., [1]). Since 1982, there are only 9 reports of human observations of tornado based on the records of the Hong Kong Observatory (HKO). The last observation dated back to 2005. Two tornado events of the 9 reports in Hong Kong have been documented in Chan et al. [2] and Kosiba et al. [3]. The former event referred to a tornado occurring over the Hong Kong International Airport with some minor damages, and the latter case covers some anticyclonic gustnadoes occurring over the southern part of the Airport. This gustnado case is one of the 9 reports, and it is regarded as tornado in Hong Kong.

According to the tornado climatology in China [4], there are 20 to 50 tornadoes over southern part of China in the period 1948 to 2012, i.e., about 0.3 to 0.8 tornado per year, and the majority of such tornadoes are weak, with the Fujita scale of 3 or below. In this region, Foshan, over southern China, is a place with rather frequent occurrence of tornado. A recent event is the tornado associated with Typhoon Mujigae in 2015. A detailed account of this event could be found in the study of Li et al. [1]. The motivation of this work is to document the environmental condition and numerical simulation of a tornado in Hong Kong, which is a rather rare event. In this case, the tornado is also not associated with a nearby tropical cyclone (e.g. [5]). The documentation hopefully would be useful for the analysis and forecast of tornado occurrence in Hong Kong in the future. In the analysis, parameters based on the sounding profiles such as wind shear [6] and Szilagyi Waterspout Index, WSI [7], would be considered.

This paper documents a case of tornado in Hong Kong at about 11:30 a.m., 29 August 2018 (in Hong Kong time, which is 8 hours ahead of UTC). There were a number of citizen reports of a waterspout to the west of Ting Kau Bridge (Figure 1(a)). The waterspout moved to the north and touched on the ground of Lido Beach, becoming a tornado (Figure 1(b)). An empty canoe on land was blown around by the swirling winds associated with the tornado. There were neither reports of casualty nor property damage. A news report of the event could be found in https://www.scmp.com/news/hong-kong/health-environment/article/2161821/waterspout-spotted-near-hong-kongs-ting-kau-bridge.

In this paper, the tornado is documented using surface observations and, in particular, the data from a Terminal Doppler Weather Radar (TDWR) at Brothers Point, Hong Kong [8], which is situated very close to the event location. Numerical simulation of the tornado would also be briefly discussed using real-time output from the aviation model (AVM) which is a super high-resolution prediction suite for modelling winds within Hong Kong [9, 10].

## 2. Data and Methodology

There is a dense network of wind measuring equipment in Hong Kong. The surface-based anemometers are distributed over the whole Hong Kong for monitoring the wind conditions in different parts of the territory. They are equipped with wind cups and vanes and normally have a height of around 10 m above the local ground as far as possible.

There is also remote sensing wind measuring equipment in Hong Kong. One is the wind profiler, such as the one located in the urban centre, which measures the horizontal wind up to about 9 km above ground (under favourable weather conditions such as rain), with the wind profile updated every 10 minutes. It uses three radar beams pointing upwards in the sky to determine the 3 components of the wind. For the airport, its wind conditions are also monitored by a Terminal Doppler Weather Radar (TDWR). This is a C-band radar that performs scanning in the airport region to measure the line-of-sight velocity component in rain. The velocity data so obtained are useful in the alerting of low-level wind shear to be encountered by the aircraft.

In the urban centre, there is also a radiosonde station located at King's Park within a few kilometres away from the wind profiler stations. Radiosondes are normally launched two to three times a day, separated by 6 to 12 hours. The radiosonde measures the upper air wind, temperature, and humidity up to 20–30 kilometres above ground. This is an important source of information about the thermodynamic conditions of the atmosphere.

## 3. Observational Results and Discussion

In the morning of 29 August 2018, the coast of southern China was under the influence of a trough of low pressure. Figure 2(a) shows the surface isobaric chart at 8 a.m. on that day. The trough of low pressure brought unsettled weather to Hong Kong, including showers and thunderstorms.

(a)

(b)

Figure 1: Photos in the morning of 29 August 2018 showing (a) the watersprout appearing at west of Ting Kau Bridge; and (b) touching down near Lido Beach as a tornado. See Figure 3 for location of these places.

The upper air radiosonde ascent in Hong Kong at 00 UTC, 29 August 2018, is shown in Figure 2(b). The atmosphere is rather humid. Instability indices are at high level: $K$ index of 37 degrees and convective available potential energy (CAPE) of 2064 J/kg which suggests a rather convective atmosphere, e.g., compared with Groenemeijer and van Delden [11]. The lower troposphere is basically uniform southwesterly winds. There is vertical wind shear between 700 and 500 hPa levels, from southwesterly wind changing to moderate easterly wind. The wind profiler observation on that day is given in Figure 2(c). The time series of vertical wind shear is given in Figure 2(d), in a way similar to the calculation of Li et al. [1]; namely, shear is calculated by considering the difference between the wind on the ground (based on Walgan Island, location in Figure 3(a)) and the

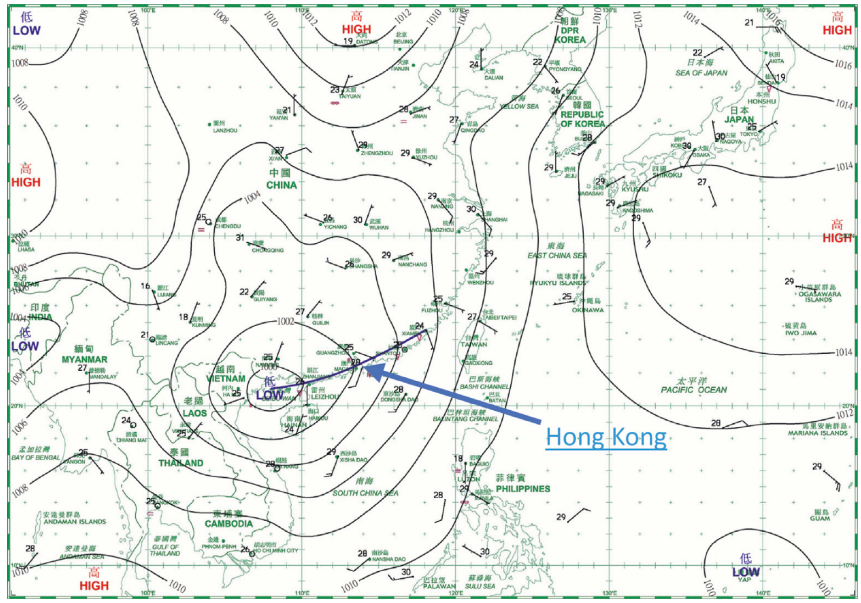


(a)

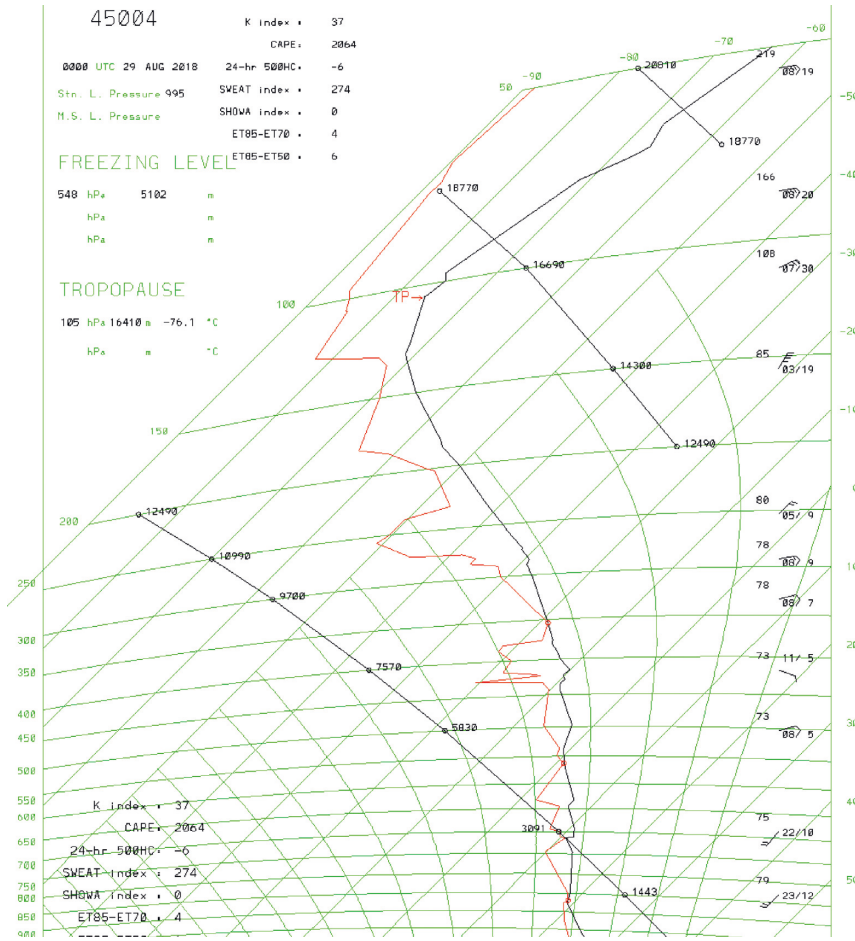


(b)

Figure 2: Continued.

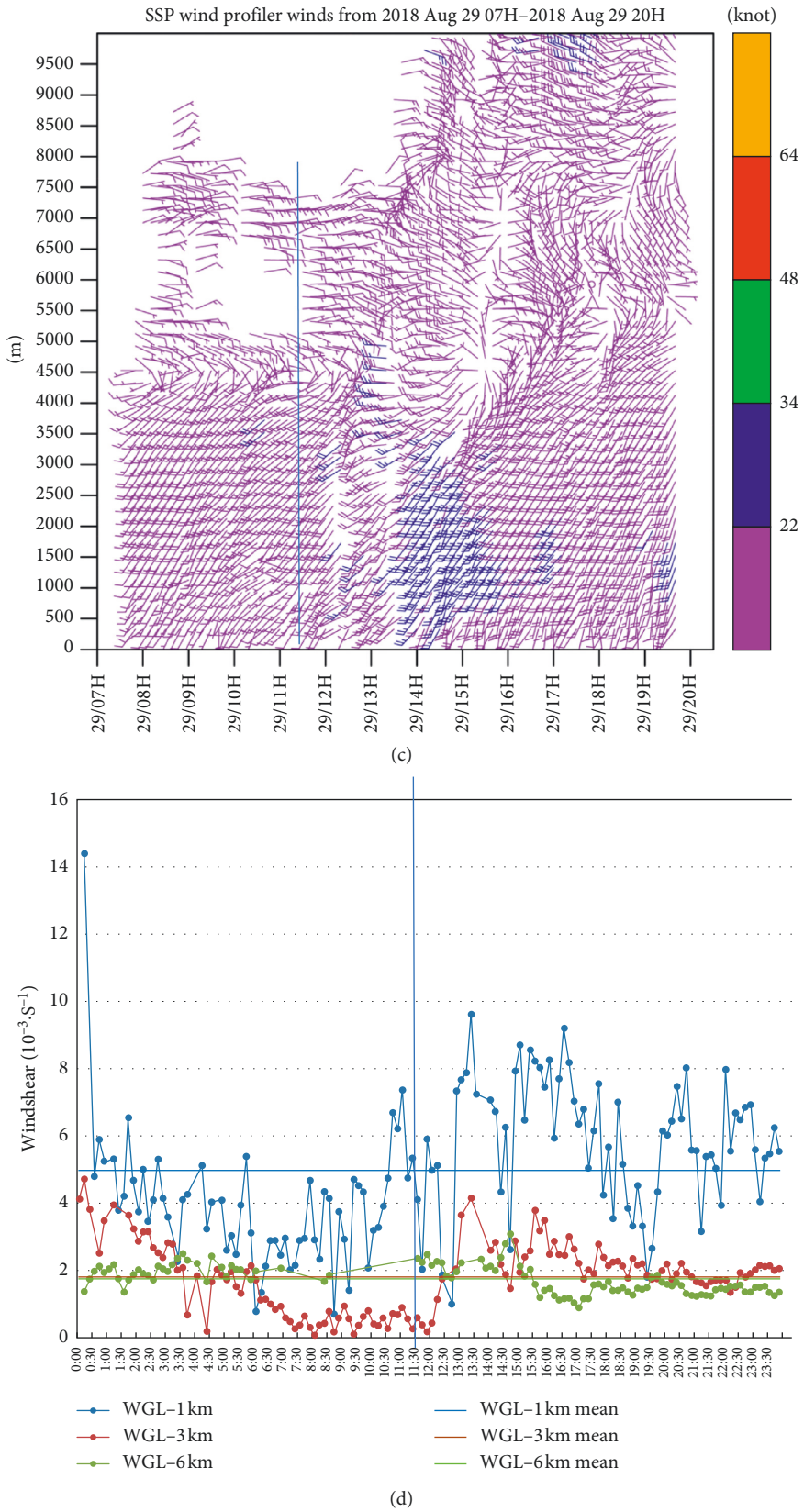


Figure 2: Various weather observations taken on 29 August 2018: (a) surface isobaric chart at 8 a.m. (local time) showing a trough of lower pressure over the coast of southern China; (b) concurrent upper-air ascent; (c) wind profiler data at a nearby urban site (time of tornado occurrence is marked with a blue line); and (d) time series of the vertical wind shear between the ground (taken to be the wind at Waglan Island) and the different heights (1 km, 3 km, and 6 km above sea level) as obtained from the wind data from the wind profiler at the urban area (the mean values are given as horizontal lines).

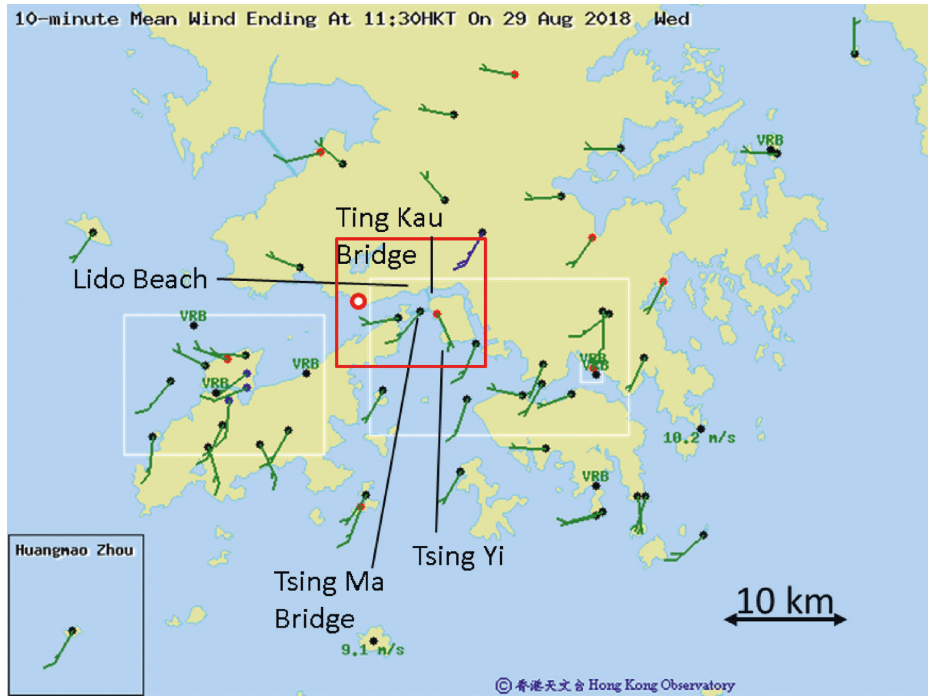


(a)

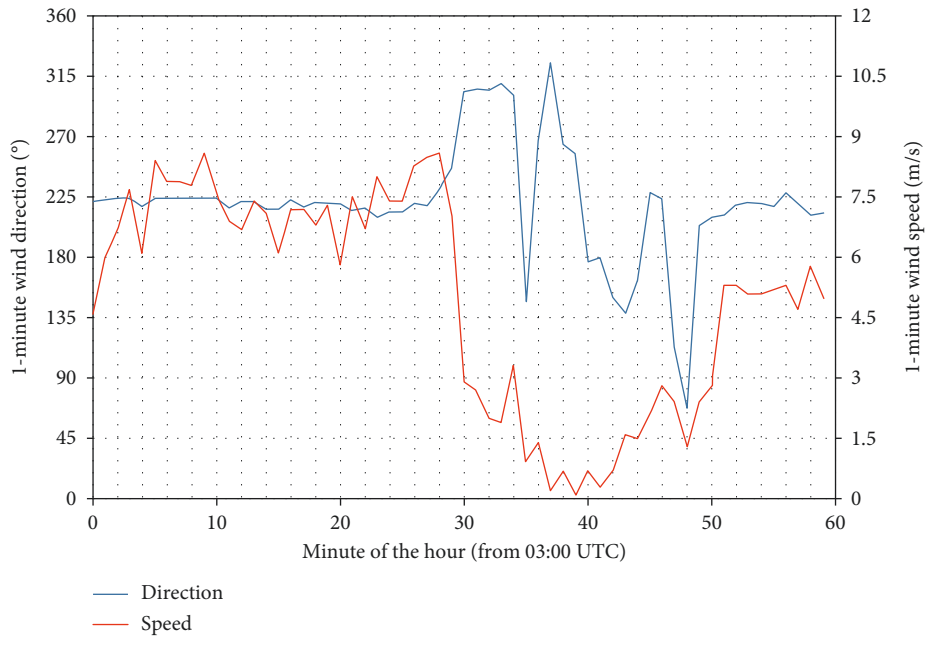


(b)

FIGURE 3: Wind observations (a) over Hong Kong during passage of the tornado with markings of key locations in this study; and (b) time series of wind speed and direction taken at the Tsing Ma Bridge during the hour of the event. Red box in (a) corresponds to the area of TDWR observations plotted in the subsequent figures.

wind at 1 km, 3 km, and 6 km above mean sea level (from the urban area wind profiler).

The vertical wind shear of 0-1 km has a mean value of about $5 \times 10^{-3}\,s^{-1}$. Before the occurrence of the tornado, the value rose to about $7.8 \times 10^{-3}\,s^{-1}$. The vertical wind shears of 0–3 km and 0–6 km are pretty small and has a mean value of about $1.9 \times 10^{-3}\,s^{-1}$ only. The 0-1 km wind shear is comparable with the values reported in the literature (e.g. [6, 11, 12]), However, the wind shears of 0–3 km and 0–6 km are very small compared with those reported in the literature.

The dynamic/thermodynamic parameters are also calculated from the 00 UTC radiosonde ascent. Following Renko et al. [7], the Szilagyi Waterspout Index (SWI) is about 10 (convective cloud depth of about 46,000 feet and the temperature difference between the sea and 850 hPa level of about 7.6 degrees). It thus supports the occurrence of

thunderstorm-related waterspout in Hong Kong. The storm relative helicity (SRH) is about 10 $m^2/s^2$ (between 0 and 3 km). This value is rather small compared with the existing literature (e.g., [12, 13]).

The surface wind observations at 11:30 a.m., 29 August 2018, are shown in Figure 3(a). The key locations of interest in this paper, including Ting Kau Bridge, Lido Beach, Tsing Ma Bridge, and Tsing Yi are shown in this figure. Also shown is the location of the TDWR whose data would be analyzed later in this paper. Unfortunately, wind data were not recorded at Ting Kau Bridge. However, as shown in the TDWR images later, the low-level meso/microcyclone associated with the tornado had once moved across Tsing Ma Bridge, and the full set of wind records was available at the centre of this bridge. The time series of wind direction and wind speed are given in Figure 3(b). It could be seen that the wind direction over there once fluctuated rapidly at about 11:30 a.m., 28 August 2018 (i.e., 30 minutes beyond 03:00 UTC, which is 11 a.m. in Hong Kong time). Wind speed was about 9 m/s at first, dropping to nearly null between 11:36 a.m. and 11:40 a.m. The wind data indicated a swirling airflow, though the wind speed was rather weak at times. This shows the presence of vortex associated with the thunderstorms near Tsing Yi at that time, though it might not be exactly the tornado as reported in the event.

Clearer signature of the presence of meso/microcyclone associated with the reported tornado comes from the Doppler velocity images of the TDWR, as shown in Figure 4. The pictures show the Doppler velocities at elevation angles of 12.5 degrees and 17 degrees from the horizon. They are roughly divided into four time slots, namely, 11:26 a.m., 11: 30 a.m., 11:35 a.m., and 11:40 a.m. The background southwesterly flow showed up in the western and northern parts of the Doppler velocity imageries, which is the background airflow. Within this background southwesterly wind, a couplet of Doppler velocity is embedded inside. Because of blockage by terrain and the implementation of sector blanking for TDWR in view of radiation safety, spatial coverage by the radar at lower elevation angels is rather limited and the velocity couplet does not show up as nicely.

There are a few observations of the characteristics of this velocity couplet:

(i) There is slight difference in the location of the couplet (highlighted using the white dotted circle) between the 12.5-degree scan and 17-degree scan at a particular time. Of course, there could be a one-minute difference between these two scans, which may contribute to the slight difference in location. However, it appears that the couplet is slanting slightly with height.

(ii) The couplet appears to move east and then northeast and eventually dissipate over the mountains.

(iii) At a particular scan, the inbound velocity (blue/green) is generally smaller than the outbound velocity (pink/red) in the couplet. This may be related to the strong background flow.

An example of the radar reflectivity imagery of the TDWR in the period of the tornado occurrence is given in Figure 5(a). It refers to the conical scan with an elevation angle of 17 degrees above horizon. The radar echo associated with the tornado does not appear to have such features as hook echo and bounded weak echo region that may be spotted in supercells. It appears as an ordinary multicellular thunderstorm only.

A vertical cross section of the Doppler velocity imagery is made at the time and place as shown in Figure 4, and the resulting cross section is given in Figure 6. There is slight counterflow between 1000 m and 2000 m above sea level at the location of the tornado. The figure also shows the blockage of the low elevation beams of the radar. There is slight tilting of the axis of the rotating flow with height.

The vertical wind profile of the tornado would be useful for the local wind engineering application, such as design of the building. The TDWR velocity data recorded in the present event provide useful information about the variation of the wind speed with height in association with the velocity couplet. Following the methodology of Snyder and Bluestein [14]; the maximum radial velocity (basically the outbound velocity as discussed above) at each elevation scan and time associated with the couplet is extracted and plotted in Figure 7. This figure shows the maximum radial velocity obtained from the different elevation scans at three different times. This is taken to be a pseudostationary structure of the tornado with negligible time difference in between, in order to display the vertical wind profile at different heights. It could be seen that the wind starts at about 10 m/s in the lowest elevation. The wind picks up relatively sharply with height between 1000 m and 2000 m above sea level, and reaches a maximum in excess of 20 m/s between 2000 m and 3000 m. This is the first time that the vertical wind profile of a tornado is obtained in Hong Kong based on the Doppler velocity measurements from a radar.

## 4. Numerical Simulation and Model Results

In the recent years, there are many numerical efforts trying to simulate the occurrence of tornado with high spatial resolution. For instance, the convective-scale ensemble forecast system for tornadogenesis has been attempted in the studies of Zhuang et al. [15] and Yussouf et al. [16]. Super high-resolution simulation of tornado occurrence (with a spatial resolution below 1 km) has been tried out in the studies of Yokota et al. [17] and Mashiko et al. [5]. However, these numerical experiments are post hoc case studies only with special focus on the occurrence of tornados. On the contrary, for the numerical model considered in the present work, it is run at super high spatial resolution (200 m) on a regular basis with the general requirement for supporting aviation weather service. It is not specifically designed for tornadogenesis experiments, e.g., no assimilation of radar data has been made (although its parent model has the benefit of indirect radar reflectivity assimilation through a 1D-VAR retrieval process). The performance of such a model in this tornado event is investigated and is expected to shed some lights on the simulation of tornado occurrence of a more "generic" numerical weather prediction model system.

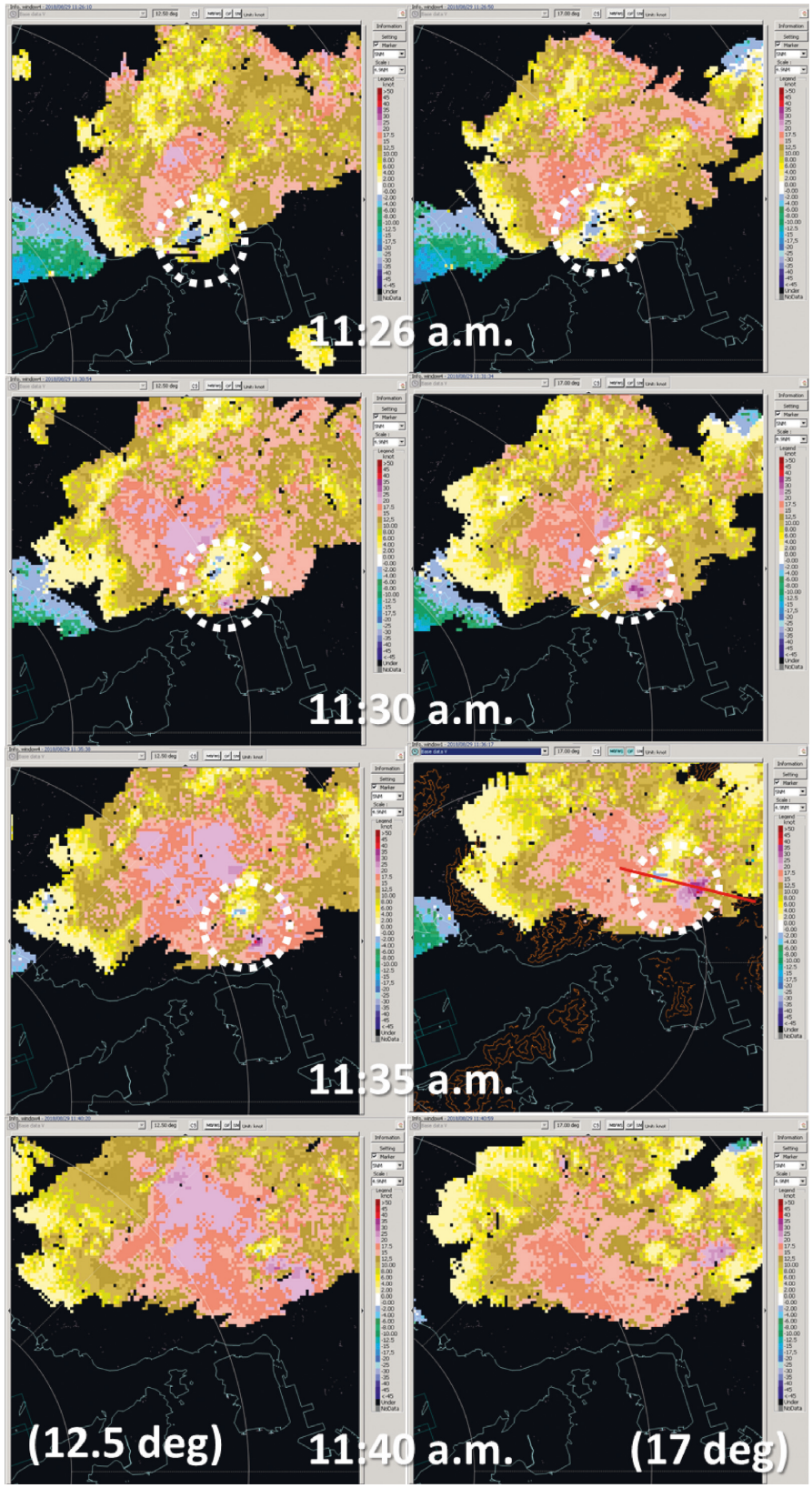


Figure 4: Sequence of Doppler velocity distribution just before and after the event as measured by 12.5 deg (left column) and 17 deg (right column) elevation scans of the TDWR. Locations of the velocity couplet, or meso/microcyclone, associated with the tornado highlighted using the dotted white circle. The domain of the current sequence is marked in red in Figure 3(a) for a better appreciation of spatial scales. The red line in the 2nd plot from the bottom in the right column marks the location of the vertical cross section shown in Figure 6.

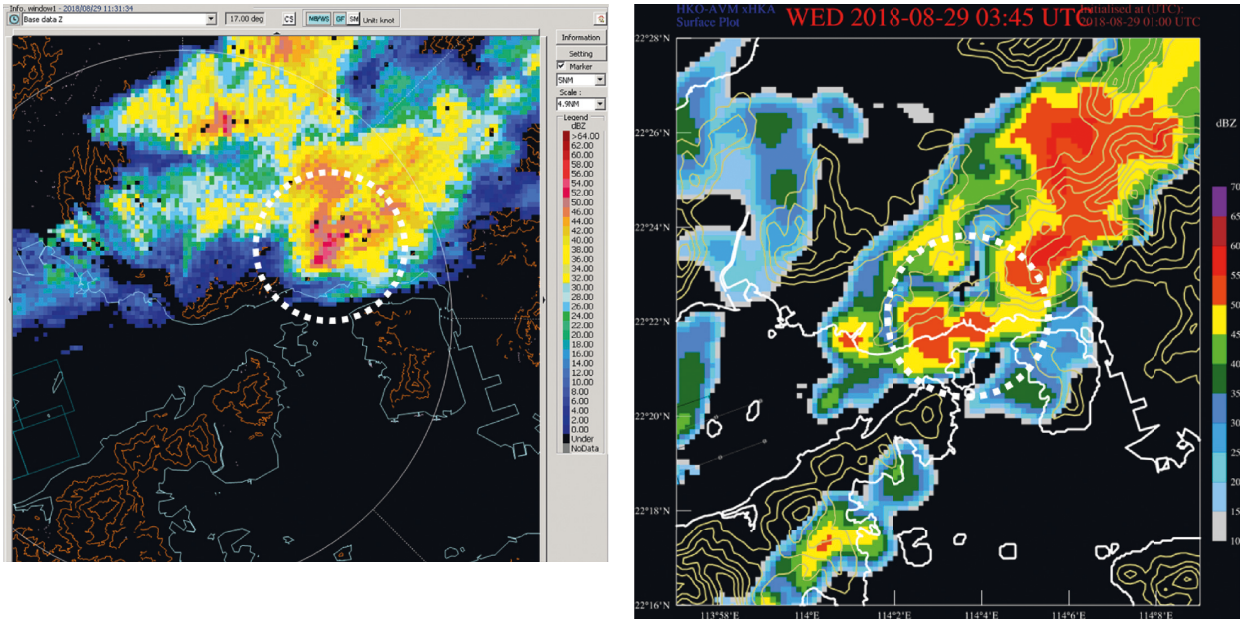


(a) (b)

Figure 5: Radar echoes associated with the thunderstorms inducing the tornado as (a) observed by the TDWR and (b) simulated by a real-time model run of the 200 m resolution AVM.

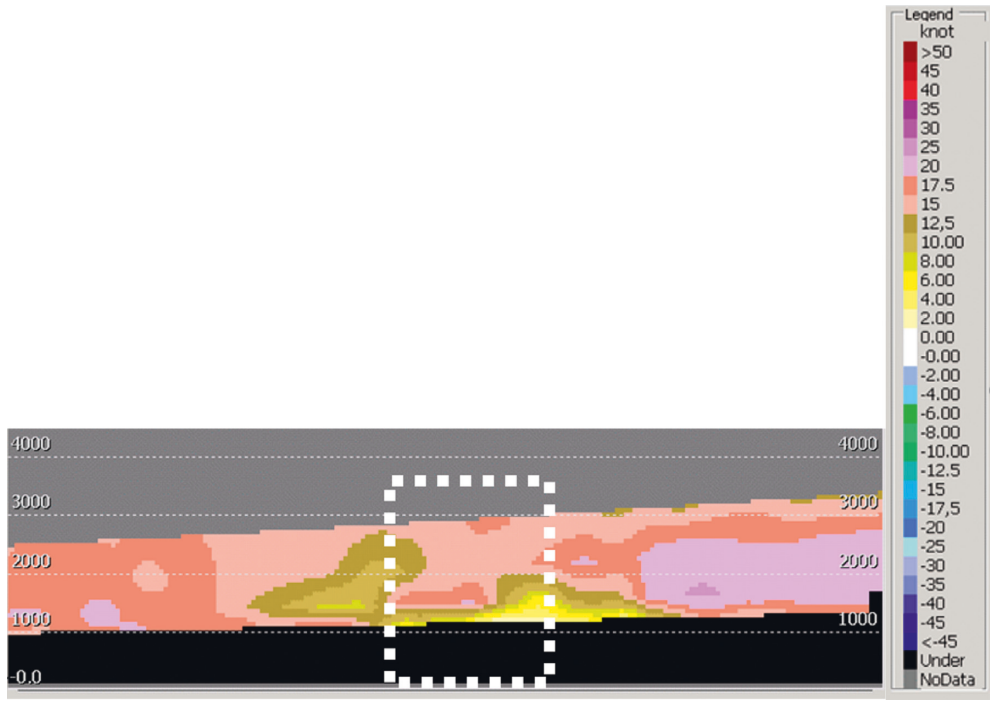


Figure 6: Cross section of Doppler velocity as taken along the red line in Figure 4 from the west to east. Location of the counterflow suggestive of rotation highlighted using the dotted white box.

The aviation model (AVM) is a subkilometre resolution implementation of the Weather Research and Forecast (WRF-ARW) model by HKO supporting fine-scale aviation weather forecasts for the Hong Kong International Airport (HKIA). The operational AVM suite comprises two singly nested domains: AVM-PRD (PRD stands for "Pearl River Delta" which is used interchangeably with "Pearl River Estuary") at 600 m resolution covering the greater Pearl River Delta (or Estuary) area and the 200 m inner domain AVM-HKA (HKA as an abbreviation of HKIA) which centres on HKIA and is recently extended to provide full coverage of the Hong Kong territory.

Both AVM-PRD and AVM-HKA domains are run on an hourly basis at HKO. Key model settings include USGS 3-

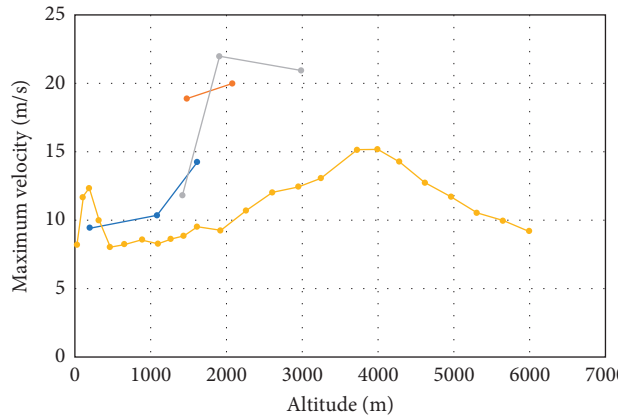


Figure 7: Maximum radial velocity with height in association with the meso/microcyclone as derived from TDWR scans (short line sections; representing different elevation angles) and 200 m resolution AVM simulations (long yellow line) following the study of Snyder and Bluestein [14].

second topography and MODIS land use, both with local adaptations, WRF double-moment 6-class microphysics scheme, the Noah land surface model, and RRTM schemes for short- and long-wave radiation. Given the high horizontal resolution, no cumulus and boundary layer parameterisation schemes are used. The AVM has demonstrated the ability to predict meso/microscale flow features associated with terrain disruption through a LIDAR simulator [9] as well as complex convective cloud distributions as viewed through simulated satellite imagery [18]. It assimilates surface wind observations, wind profiler data, and aircraft winds only. However, it does not utilise weather radar observations. As a result, it relies partly on initial fields from the parent 2 km mesoscale model for various hydrometeors in reproducing the observed thunderstorms in the current case.

The real-time model run initialized at 01 UTC, 29 August 2018, is considered in this paper. The simulated radar echo distributions from the 2 hour 45 minute forecast (i.e., valid at 03:45 UTC) is given in Figures 5(b) and 8(b) and compared with the TDWR and Tai Mo Shan weather radar (location in Figure 3(a)) reflectivity observations. The output time of 03:45 UTC is chosen after detailed inspection of AVM forecast fields at 1-minute output intervals. It is used to compare against radar observations at 03:30 UTC, which implies a time delay of about 15 minutes in the AVM prediction of the event.

It could be seen that there is a southwest-northeast oriented band of rain cells over the western and central parts of Hong Kong. The surface wind barbs are given in Figure 8(b). It could be seen that, inside this rain band, there are some small surface vortices embedded. For more direct comparison with the TDWR data, the reflectivity and velocity are plotted in the respective scales of this radar, and the results are given in Figures 5 and 9, respectively. It could be seen from Figure 5(a) that the rain appears to be associated with multicellular storms. The forecast radar reflectivity distribution is correct in that there are no features such as hook echo and weak echo region in association with supercells, which have been demonstrated to be resolvable by NWP models at similar or even coarser spatial resolutions (e.g., [19, 20]). In Figure 9(b), the full 3-dimensional wind components are used to compute the simulated Doppler velocity fields as would be observed by a 17-degree elevation scan of the TDWR. Comparing with Figure 9(a), both figures bear similar features like the background southwesterly flow and the presence of an elongated region with opposing flow (inbound velocity of white and outbound velocity in pink and brown). Inside this elongated region, some low-level vortices are embedded inside.

A vertical cross section is made along the red line shown in Figure 9(b), and the resulting plots are shown in Figure 10 (south-north direction in Figure 9(b) is displayed from left to right in Figure 10). In these plots, the location of the simulated cyclone feature is marked in black. It could be seen that there is a region of opposing velocities for both $U$ (east-west component of the wind; Figure 10(a)) and $V$ (north-south component of the wind; Figure 10(b)) in the highlighted region. A small cyclone is embedded inside this region of higher simulated reflectivity (as revealed in Figure 5(b)). The vertical cross sections of $W$ (vertical velocity) and $Q_{\text{cloud}}$ (cloud liquid water content) are shown in Figures 10(c) and 10(d), respectively. At the location of the small cyclone, there is strong updraft with a core around 2500 m above the mean sea level and a region with the higher amount of liquid water content descending from a maximum at around 2000 m above the mean sea level. Considering the various simulated quantities, the AVM is considered to have successfully predicted the presence of a meso/microcyclone in association with the tornado in a real-time setting. While the simulated cyclone features (including descending $Q_{\text{cloud}}$) did not penetrate sufficiently close to ground or sea level to produce exactly a tornado, the simulated vertical structure between 1000 m and 4000 m appears in line with other real-time sub-kilometric resolution results [20]. Moreover, the slightly tilted structure of the simulated cyclone also corresponds to TDWR observations.

As a further comparison, the maximum radial velocity at the various heights in association with the simulated

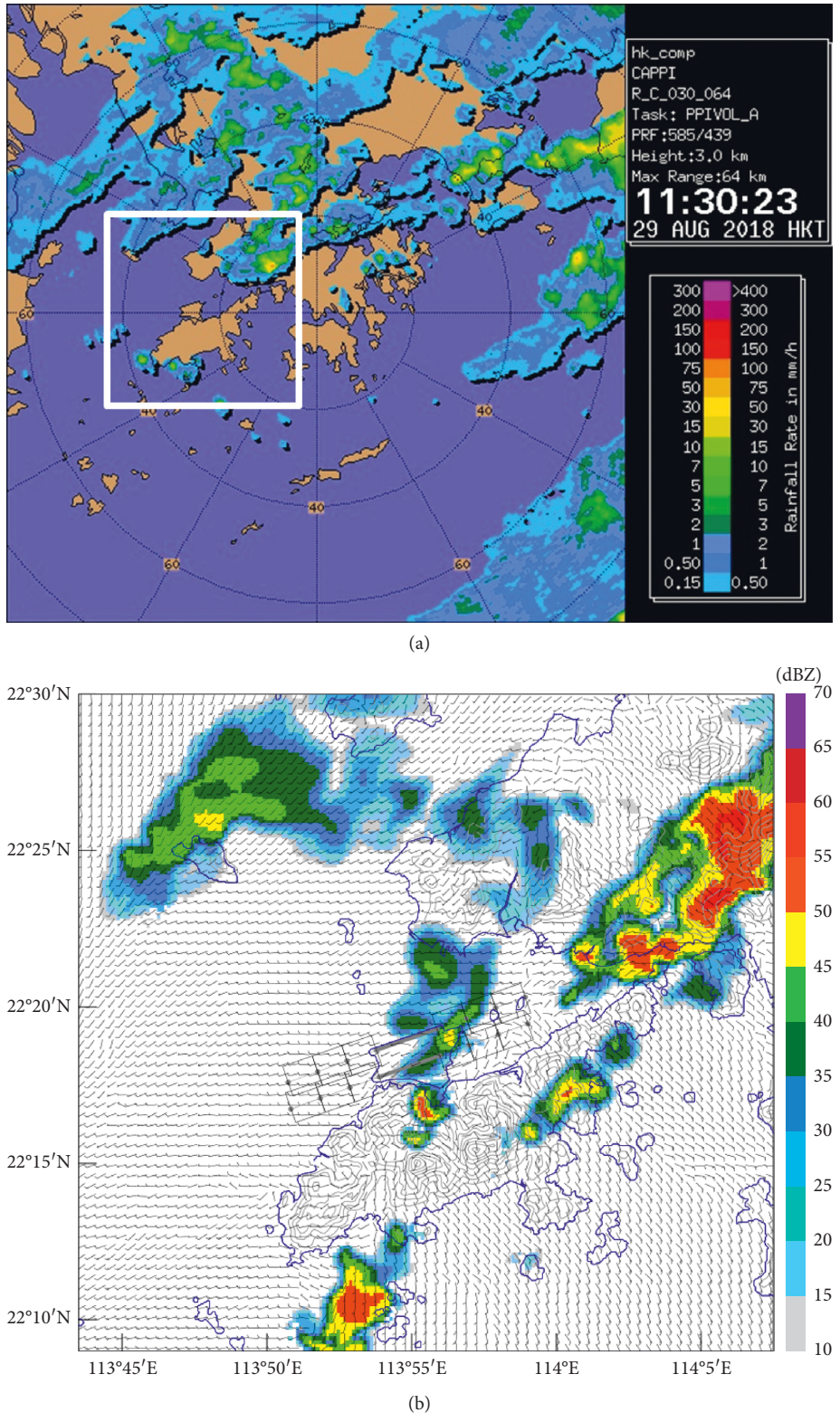


Figure 8: Distribution of radar echoes around Hong Kong as (a) observed by 3 km constant-altitude display of the Tai Mo Shan weather radar of HKO and (b) predicted by 200 m resolution AVM. The plotted area of (b) is marked by the white square in (a).

velocity couplet is extracted and plotted together with the actual observation from the radar in Figure 7. The two graphs show some similarity, namely, the gradual rise of velocity from 1000 m to 3000–4000 m, though the highest value of the maximum radial velocity and the height of occurrence are a bit different. Also, the model simulation

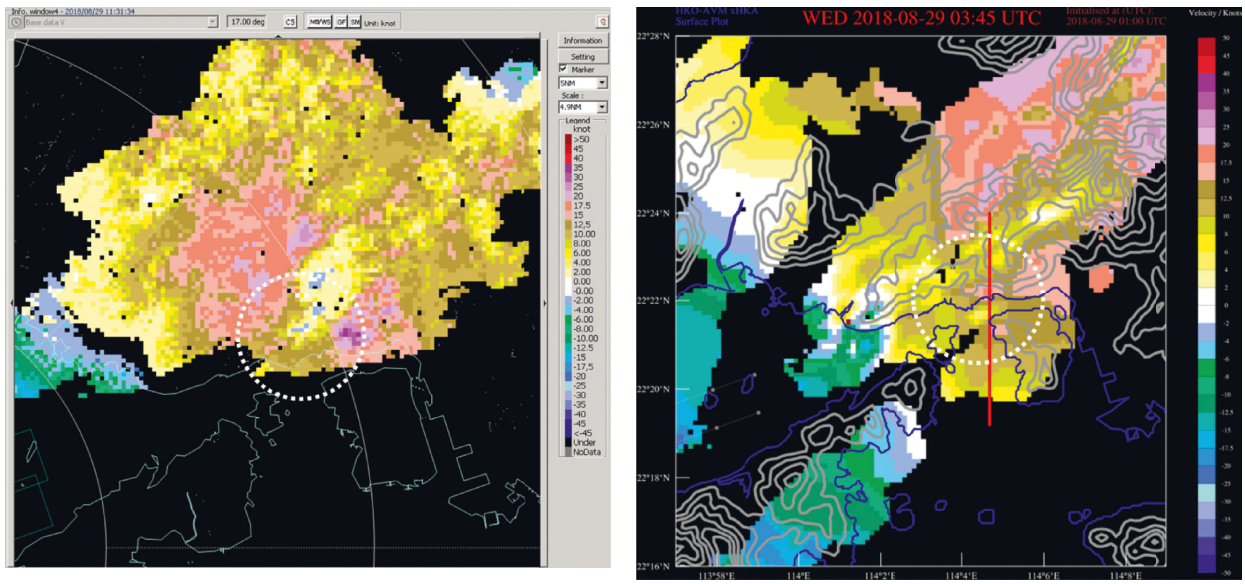


(a) (b)

Figure 9: Doppler velocity distribution as (a) observed by the TDWR on a 17-deg elevation scan and (b) predicted by the 200 m AVM. Location of the key rotating circulation is marked in white in each case. Cross sections in Figure 10 below are taken along the red line marked in (b).

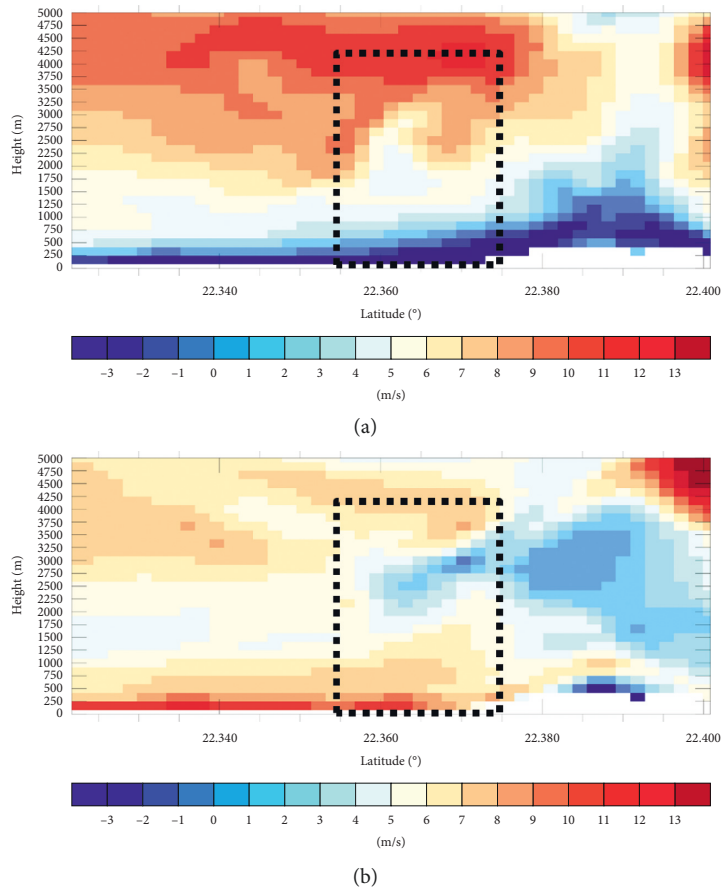


(a)

(b)

Figure 10: Continued.

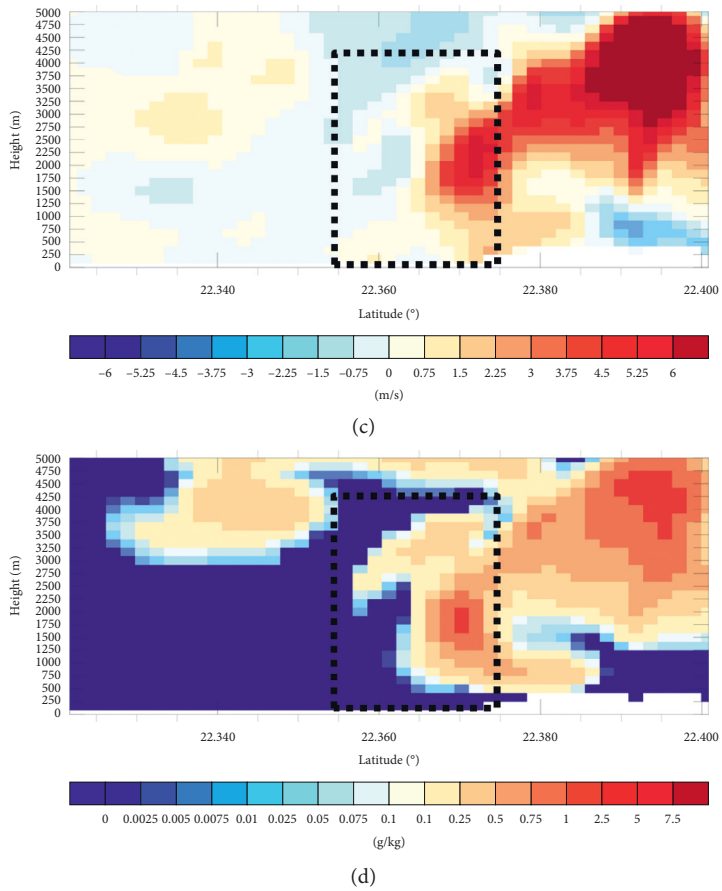


Figure 10: Cross section along the red line marked in Figure 9(b) (south-north direction appearing from left to right here) based on 200 m AVM simulations of (a) $U$; (b) $V$; (c) $W$; (d) $Q_{\text{cloud}}$. Location of simulated cyclone feature highlighted using the dotted black box. Note the asymmetric colour scale (i.e., not centered at zero) used in both (a) and (b) to suppress visual effects of the prevailing southwesterly background wind flow.

shows slightly higher radial velocity at a height of about 200–300 m, which was not present in the TDWR observations. This may be due to blanking of the radar beam, and thus, limitations in capturing the higher value of radial velocity in the lowest part of the meso/microcyclone are closer to surface.

## 5. Conclusion

This paper documents the observational data in a tornado case in Hong Kong, which is a rather rare weather event. The meso/microcyclone associated with the tornado is well captured by the TDWR. For the first time, the vertical profile of maximum radial velocity is obtained for this tornado, and the information would be useful for wind engineering applications in Hong Kong. The analysis of Doppler velocity from a weather radar is a special feature of the present study in the southern China region, e.g., in comparison with other tornado studies in this region such as the study of Li et al. [1].

Real-time runs of the 200 m resolution AVM of HKO appear to be capable in capturing the meso/microcyclone signature. The vertical cross section across the cyclone helps us to reveal the interesting features in line with literature results which are not easily observable by conventional instruments or methods, such as vertical velocity and cloud liquid water content. Also, the simulated vertical profile of maximum radial velocity is similar to the actual observations. The routine operation of a high-resolution NWP model is a special feature of this study, in comparison with the previous dedicated experiments such as the studies of Mashiko et al. [5] and Yokota et al. [17].

Similar to other studies such as those of Groenemeijer and van Delden [11] and Renko et al. [7], proximity sounding has been analyzed to show the background dynamic and thermodynamic of the atmosphere for the occurrence of the tornado.

The results in this paper are considered to be a useful reference not just for Hong Kong but also elsewhere in the world in further understanding the internal structure of a tornado and also demonstrate the power of very high-resolution NWP models in predicting such events even in a real-time fashion.

## Data Availability

The data used to support the findings of this study may be available from the corresponding author upon request.

## Conflicts of Interest

The authors declare that there are no conflicts of interest regarding the publication of this paper.

## Acknowledgments

Mr. Tobias Chan is gratefully acknowledged for providing the photo in Figure 1(a) and Hong Kong Government Lifeguards General Union for Figure 1(b). The authors thank Mr. F. M. H. Lee of the Chinese University of Hong Kong for preparation of graphics.

## References

[1] Z. Li, D. Wang, X. Mai et al., "Observations of the tornado occurred at Foshan on 4 October 2015," *Acta Meteorologica Sinica*, vol. 75, pp. 288–313, 2017, in Chinese.

[2] P. W. Chan, J. Wurman, C. M. Shun, P. Robinson, and K. Kosiba, "Application of a method for the automatic detection and ground-based velocity track display (GBVTD) analysis of a tornado crossing the Hong Kong International Airport," *Atmospheric Research*, vol. 106, pp. 18–29, 2012.

[3] K. A. Kosiba, P. Robinson, P. W. Chan, and J. Wurman, "Wind field of a nonmesocyclone anticyclonic tornado crossing the Hong Kong International Airport," *Advances in Meteorology*, vol. 2014, Article ID 597378, 7 pages, 2014.

[4] J. Chen, X. Cai, H. Wang et al., "Tornado climatology of China," *International Journal of Climatology*, vol. 38, no. 5, pp. 2478–2489, 2017.

[5] W. Mashiko, H. Niino, and T. Kato, "Numerical simulation of tornadogenesis in an outer-rainband minisupercell of typhoon Shanshan on 17 September 2006," *Monthly Weather Review*, vol. 137, no. 12, pp. 4238–4260, 2009.

[6] W. Pilorz, I. Laskowski, E. Łupikasza, and M. Taszarek, "Wind shear and the strength of severe convective phenomena-preliminary results from Poland in 2011–2015," *Climate*, vol. 4, no. 4, p. 51, 2016.

[7] T. Renko, S. Ivusic, M. T. Prtenjak, V. Solian, and I. Horvat, "Waterspout forecasting method over the eastern Adriatic using a high-resolution numerical weather model," *Pure and Applied Geophysics*, vol. 175, no. 11, pp. 3579–3778, 2018.

[8] S. M. Tse, "Optimization of terminal Doppler weather radar at Hong Kong international airport for microburst detection," in *Proceedings of 9th European Conference on Radar and Meteorology and Hydrology*, Antalya, Turkey, October 2016.

[9] P. W. Chan and K. K. Hon, "Performance of super high resolution numerical weather prediction model in forecasting terrain-disrupted airflow at the Hong Kong International Airport: case studies," *Meteorological Applications*, vol. 23, no. 1, pp. 101–114, 2015.

[10] W.-K. Wong, C.-S. Lau, and P.-W. Chan, "Aviation model: a fine-scale numerical weather prediction system for aviation applications at the Hong Kong International Airport," *Advances in Meteorology*, vol. 2013, Article ID 532475, 11 pages, 2013.

[11] P. H. Groenemeijer and A. van Delden, "Sounding-derived parameters associated with large hail and tornadoes in The Netherlands," *Atmospheric Research*, vol. 83, no. 2–4, pp. 473–487, 2007.

[12] O. Rodríguez and J. Bech, "Sounding-derived parameters associated with tornadic storms in Catalonia," *International Journal of Climatology*, vol. 38, no. 5, pp. 2400–2414, 2017.

[13] R. L. Thompson, R. Edwards, J. A. Hart, K. L. Elmore, and P. Markowski, "Close proximity soundings within supercell environments obtained from the rapid update cycle," *Weather and Forecasting*, vol. 18, no. 6, pp. 1243–1261, 2003.

[14] J. C. Snyder and H. B. Bluestein, "Some considerations for the use of high-resolution mobile radar data in tornado intensity determination," *Weather and Forecasting*, vol. 29, no. 4, pp. 799–827, 2014.

[15] Z. Zhuang, N. Yussouf, and J. Gao, "Analyses and forecasts of a tornadic supercell outbreak using a 3DVAR system ensemble," *Advances in Atmospheric Sciences*, vol. 33, no. 5, pp. 544–558, 2016.

[16] N. Yussouf, E. R. Mansell, L. J. Wicker, D. M. Wheatley, and D. J. Stensrud, "The ensemble Kalman filter analyses and forecasts of the 8 May 2003 Oklahoma city tornadic supercell storm using single- and double-moment microphysics schemes," *Monthly Weather Review*, vol. 141, no. 10, pp. 3388–3412, 2013.

[17] S. Yokota, H. Seko, M. Kunii, H. Yamauchi, and H. Niino, "The tornadic supercell on the Kanto plain on 6 may 2012: polarimetric radar and surface data assimilation with EnKF and ensemble-based sensitivity analysis," *Monthly Weather Review*, vol. 144, no. 9, pp. 3133–3157, 2016.

[18] K. K. Hon, "Simulated satellite imagery at sub-kilometre resolution by the Hong Kong Observatory," *Weather*, vol. 73, no. 5, pp. 139–144, 2018.

[19] D. C. Dowell, L. J. Wicker, and C. Snyder, "Ensemble Kalman filter assimilation of radar observations of the 8 May 2003 Oklahoma City supercell: influences of reflectivity observations on storm-scale analyses," *Monthly Weather Review*, vol. 139, no. 1, pp. 272–294, 2011.

[20] K. E. Hanley, A. I. Barrett, and H. W. Lean, "Simulating the 20 May 2013 Moore, Oklahoma tornado with a 100-metre grid-length NWP model," *Atmospheric Science Letters*, vol. 17, no. 8, pp. 453–461, 2016.